SURFACE PLASMON ENHANCED OPTICAL FORCES in NANOSTRUCTURES and WAVEGUIDES

by

Aybike Ural Yalçın

A Thesis Submitted to the
Graduate School of Sciences and Engineering
in Partial Fulfillment of the Requirements for
the Degree of

Master of Science

in

Physics

Koç University

September, 2013

Koç University

Graduate School of Sciences and Engineering

This is to certify that I have examined this copy of a master's thesis by

Aybike Ural Yalçın

and have found that it is complete and satisfactory in all respects,
and that any and all revisions required by the final
examining committee have been made.

Chair of Supervisory Committee:

Reading Committee:

_____

Assist. Prof. Kaan Güven

_____

Prof. Dr. Özgür E. Müstecaplıoğlu

_____

Assist. Prof. Şükrü Ekin Kocabaş

Date: _____

TABLE OF CONTENTS

LIST OF FIGURES

ABSTRACT

The utilization of optical forces at the nano-scale is progressing rapidly following their successful employment in controlling micro-scale particles through optical traps and tweezers. Unlike the micro-scale, the nano-scale resides in the deep subwavelength limit, and thus, cannot benefit from the simple ray-optics based formulations. Furthermore, the interaction of light with subwavelength structures is in general poor, unless the structure possesses metallic behavior to harness surface-plasmons for efficient coupling to light. This, in turn, requires the formulation of near field electrodynamics by taking the surface-plasmon excitations into account. These major points drive the basic research on the physics of optical forces at nanoscale for demanding biomedical, chemical and integrated photonic applications.

In this thesis work, we investigate the optical forces in two different systems: (i) The surface-plasmon enhanced optical forces on illuminated nanorod pairs, and (ii) the optical forces between coupled dielectric and metal-strip waveguides. We use a theoretical/numerical framework to study the electrodynamics of optical forces starting from Maxwells equations and the Maxwell Stress Tensor. In the first system, we determine the frequency spectrum of the optical force in a range where the surface-plasmon resonance of the metal is present. In particular, we address the problem of tunability of the generated optical force and demonstrate that this is possible by incorporating a dielectric interlayer with tunable index of refraction (e.g. liquid crystal). The effect of permittivity and dielectric layer thickness on the common and relative forces are investigated in detail.

For the coupled waveguides, we start with the coupled mode theory and obtain the modes of parallel dielectric waveguides. The mode profiles are used to determine the lateral stress on the waveguides. By incorporating a simple mechanical

model, the structural deformation of the waveguide is obtained. Next, we set-up the model of plasmonic metal-strip waveguides in order to investigate the effect of surface-plasmons.

ÖZETÇE

Mikro ölçekteki parçacıkların optik tuzak ve cımbızlarla başarılı bir şekilde kontrolünü takiben, optik kuvvetlerin nano ölçekte kullanımı da hızla gelişmektedir. Mikro ölçeğin aksine, nano-ölçek dalgaboyu-altı limitinde yer aldığından, geometrik optiğe dayalı formülasyondan yararlanamamaktadır. Buna ek olarak, ışığın dalgaboyu altı yapılarla etkileşimi genelde zayıftır, ancak yüzey plazmonlarının uyarılabildiği metalik özellikleri taşıdığı taktirde bu etkileşim güçlenebilir. Böylece yüzey plazmonlarının uyarılmalarını dikkate alarak yakın alan elektrodinamiği formülasyonu gerekmektedir. Bu başlıca noktalar, nano ölçekte optik kuvvetlerin biyomedikal, kimyasal ve tümleşik fotonik uygulamalarda kullanılmak üzere temel bilimsel araştırmalarına gereksinim oluşturmaktadır.

Bu tez çalışmasında, iki farklı sistemde optik kuvvetleri araştırıyoruz: (i) Yüzey plazmon ile kuvvetlendirilmiş nanoçubuk çifti üzerinde optik kuvvetler, ve (ii) çift dielektrik ve metal şerit dalga kılavuzları arasındaki optik kuvvetler. Maxwell denklemlerinden başlayarak ve Maxwell stress tensöründen yararlanarak optik kuvvetlerin elektrodinamiğini çalışmak için teorik ve numerik yaklaşım kullandık. İlk sistemde, metalin yüzey plasmon resonansının bulunduğu bir aralıkta optik kuvvetin frekans spektrumu belirlendi. Özellikle, oluşan optik kuvvetin ayarlanabilmesi problemi üzerinde duruldu ve değişken kırılma indisine sahip (likit kristal) bir dielektrik ara katman koyarak yapılabileceği gösterildi. Yalıtkanlık sabitinin ve dieletrik katmanın kalınlığının ortak ve relatif kuvvetler üzerindeki etkileri detaylı olarak incelendi.

İkincil olarak, çift dielektrik dalga kılavuzlarının modlarını elde ettik. Mod profillerine bağlı dalga kılavuzları üzerindeki yanal stresi belirleyerek dalga kılavuzlarının yapısal deformasyonunu elde ettik. Sonrasında, yüzey plazmonlarının etkilerini araştırmak için plazmonik metal şerit dalgakılavuzları modelini oluşturduk.

ACKNOWLEDGEMENT

First of all, I would like to thank my advisor Asst. Prof. Kaan Güven for his guidance, patience and support throughout this work. I am grateful for all his explanations, answers and knowledge sharing.

I would like to thank also my thesis committee members Prof. Dr. Özgür Müstecaplıoğlu and Asst. Prof. Dr. Şükrü Ekin Kocabaş for their advice, suggestions and crucial contributions.

I acknowledge TUBITAK for providing the scholarship under the national graduate scholarship program supporting the reseach and my graduate study.

Chapter 1

INTRODUCTION

The earliest direct manifestation of the optical forces was reported by the astronomers when they noticed that the tails of comets always point away from the Sun along their trajectory. The radiation pressure exerted by light is responsible for this observation. Study on electromagnetic fields and radiation shows that light has momentum and thus can exert pressure on objects [1]. Solar sail is also proposed [2] as a possible way for space voyage using solar radiation pressure. The optical forces exerted by light is also signifcant at very small scales [3]. Optical forces can be classified as gradient and scattering forces which are reported by Ashkin et al. on micron sized particles in 1970 [4]. Their studies led to the first demonstration of an optical tweezer for stable control of particles in free space [5]. While the dielectric particles are attracted along the electric field gradient to the region of strongest electric field, the scattering force is acting on the particles along the direction of light propagation as shown in Fig.1 of ref. 1.1. The time-averaged scattering and gradient forces on a sphere illuminated by a time-harmonic electromagnetic field are calculated in [6]. The time-averaged force expression in terms of the particle polarizability is shown to be the total force which carries both the gradient and scattering force, and it gives only the scattering force in the case of a plane wave illumination.

The contribution of surface plasmons (SPs) can not be neglected in calculations of optical forces on conducting particles. Optical forces are enhanced due to field enhancement near the structures as metal spheres, cylinders at their surface plasmon

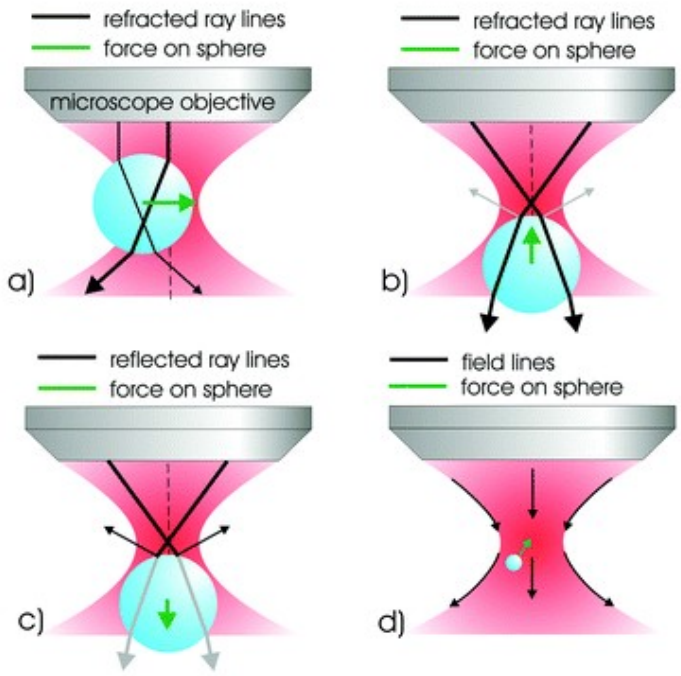

Figure 1.1: Optical trapping is shown using ray-optics. (a) The focused light is refracted through the transparent particle and imparts momentum to the particle which conserves the change in direction experienced by the light. The particle moves under this action until it reaches an equilibrium position at the centre of the symmetric beam. Similar ray-tracing arguments (b) may be applied to predict the stable trapping position in the z-direction near the focus. Additionally radiation pressure (c) tends to destabilise the trap moving the particle along the propagation direction. For the Rayleigh particles (d) the polarisability of the particle is important for optical trapping . The electric field of the light produces an induced dipole in the particles which align to regions of high field gradient (in the static field approximation) [35].

resonances [7, 8, 9, 10]. Other than the gold nanospheres or nanorods coupled to a gold slab [11, 12], the optical forces on dielectric, plasmonic and hybrid waveguides are also studied [13, 14, 15, 16, 17]. In hybrid plasmonic waveguides, optical force is shown to be stronger than the optical force created in a dielectric waveguide on a dielectric substrate. The optical force enhancement in integrated metal-dielectric hybrid plasmonic waveguide is demonstrated experimentally in ref. [17] and results confirmed the optical force enhancement. Then optical force is also investigated on a metamaterial film attracted to a dielectric surface exceeding the radiation pressure[18]

or on the waveguides combined with metamaterials [19] showing enhanced optical gradient force between the waveguides.

Optical forces are utilized growingly in biomedical, chemical, integrated photonic applications [20, 21, 22, 23]. In biological studies, optical forces demonstrate themselves as optical tweezers which have a significant role to investigate the properties of DNA, proteins, cells. Optical traps open the way of manipulation and control the position of micro/nano-particles for the fabrication of photonic crystals, for the transportation in the integrated photonic device or for the creation of a crystalline structure [24, 25, 26]. Optical fields can also induce significant forces between microscopic aggregates of dielectric matter. The researchers have shown that micron (and submicron) particles in colloidal suspensions can be controlled and ordered on being illuminated by a laser beam [26, 27]. The scattering force which is parallel to the direction of radiation propagation is employed in cavity optomechanics in cooling the mechanical oscillator [29]. Plasmonic resonance dependence on the particle size is used in optical sorting of nanoparticles as an application of optical forces taking the advantage of plasmonic fields [28].

Optical forces are also considered between coupled waveguides. The gradient optical forces are exploited for all-optical actuation of nanomechanical systems such as waveguides, integrated resonators resulting in nanometre level displacements [14, 20, 21, 30]. The freely-hanging coupled dielectric waveguides are studied experimentally [13, 31]. They showed that the sign of the force applied by one waveguide to the other can be tuned from attractive to repulsive by controlling the relative phase of the optical fields injected into the waveguides. Moreover, using resonant structures the effect of the optical forces enhanced as shown by Anetsberger et al [32]. Also, the forces arising from coupled surface plasmon polaritons in planar waveguides composed of a finite or infinite thick metal slab separated by air are studied [33].

In this thesis, we investigate tailoring the magnitude and direction of the surface-

plasmon enhanced optical forces. The optical forces between gold, silver nanoparticles and nanorods are explored in recent studies [8, 9, 10, 36]. We investigate the effect of a dielectric interlayer incorporated between the gold nanorods.

The thesis is organized as follows: The second chapter presents the theoretical formulation of the optical forces in terms of the Maxwell stress tensor and it shows the scattering and gradient forces in the dipole approximation. The third chapter begins with a brief introduction on the theory of surface plasmons and then presents the main outcomes of this study. We characterize the optical force with respect to the parameters of the dielectric slab. We also discuss the tunability of the optical force by a liquid crystal dielectric slab for dynamic control. The fourth chapter is devoted to the optomechanical forces between coupled waveguides. We present briefly the coupled mode theory of the waveguides and calculate the optical forces generated by the coupled modes. The resulting spatial displacement of the waveguides are also calculated by employing a structural mechanics model.

Chapter 2

OPTICAL FORCES

2.1 The Maxwell stress tensor

Both the gradient and scattering type optical forces can be calculated using the Maxwell stress tensor formalism. In the following, we briefly present the derivation of the Maxwell's stress tensor starting from Maxwell's equations and formulate the optical force, as can be found in standart electrodynamics textbooks [1].

$$\nabla \cdot \mathbf{E} = 4\pi\rho \tag{2.1}$$

$$\nabla \cdot \mathbf{B} = 0 \tag{2.2}$$

$$\nabla \times \mathbf{E} = -\frac{1}{c}\frac{\partial \mathbf{B}}{\partial t} \tag{2.3}$$

$$\nabla \times \mathbf{B} = \frac{4\pi}{c}\mathbf{j} + \frac{1}{c}\frac{\partial \mathbf{E}}{\partial t} \tag{2.4}$$

From the Lorentz force, we can define the force density f, then total force in a volume V will be

$$\mathbf{f} = \rho\mathbf{E} + \frac{1}{c}\mathbf{j} \times \mathbf{B} \tag{2.5}$$

$$\mathbf{F} = \int_V [\rho\mathbf{E} + \frac{1}{c}\mathbf{j} \times \mathbf{B}]dV \tag{2.6}$$

We can eliminate ρ and $\mathbf{j}$ using Maxwell equations(1st and 4th)

$$\mathbf{f} = \frac{1}{4\pi}[\mathbf{E}(\nabla \cdot \mathbf{E}) + \frac{1}{c}\mathbf{B} \times \frac{\partial \mathbf{E}}{\partial t} - \mathbf{B} \times (\nabla \times \mathbf{B}) \tag{2.7}$$

Now, we can write that

$$\frac{\partial}{\partial t}(\mathbf{E} \times \mathbf{B}) = \left(\mathbf{E} \times \frac{\partial \mathbf{B}}{\partial t}\right) - \left(\mathbf{B} \times \frac{\partial \mathbf{E}}{\partial t}\right) \tag{2.8}$$

and we obtain

$$\mathbf{f} = \frac{1}{4\pi}[\mathbf{E}(\nabla \cdot \mathbf{E}) + \mathbf{B}(\nabla \cdot \mathbf{B}) - \mathbf{E} \times (\nabla \times \mathbf{E}) - \mathbf{B} \times (\nabla \times \mathbf{B})] - \frac{1}{4\pi c}\frac{\partial}{\partial t}(\mathbf{E} \times \mathbf{B}) \tag{2.9}$$

The i^{th} component of the following expression can be written as

$$[\mathbf{E}(\nabla \cdot \mathbf{E}) - \mathbf{E} \times (\nabla \times \mathbf{E}]_i = \sum_j \frac{\partial}{\partial j}(E_i E_j - \frac{1}{2}\mathbf{E} \cdot \mathbf{E}\delta_{ij}) \tag{2.10}$$

At this stage we introduce the Maxwell stress tensor as follows

$$T_{i\,j} = \frac{1}{4\pi}[(E_i E_j - \frac{1}{2}\delta_{i\,j}E^2) + (B_i B_j - \frac{1}{2}\delta_{i\,j}B^2)] \tag{2.11}$$

where $\delta_{i\,j}$ is the Kronecker delta and the indices i, j are space coordinates (x, y, z). Force per unit volume can be written as

$$\mathbf{f} = \nabla \cdot \overleftrightarrow{\mathbf{T}} - \frac{1}{4\pi c}\frac{\partial}{\partial t}(\mathbf{E} \times \mathbf{B}) \tag{2.12}$$

Then the total force on the charges in the volume V is given by

$$\mathbf{F} = \int_V \nabla \cdot \overleftrightarrow{\mathbf{T}} dV - \frac{1}{4\pi c}\frac{d}{dt}\int_V (\mathbf{E} \times \mathbf{B}) dV \tag{2.13}$$

The volume integral of the first term can be converted to a surface integral using the divergence theorem, so the mechanical force is equal to

$$\mathbf{F} = \oint_{\partial V} \overleftrightarrow{\mathbf{T}} \cdot \mathbf{n} da - \frac{1}{4\pi c}\frac{d}{dt}\int_V (\mathbf{E} \times \mathbf{B}) dV \tag{2.14}$$

where ∂V denotes the surface enclosing the volume V, $\mathbf{n}$ is the unit vector perpendicular to the surface, da is the infinitesimal area element, and the second term of the equation 2.14 is proportional to the Poynting vector $\mathbf{S} = \frac{c}{4\pi}(\mathbf{E} \times \mathbf{H})$.

We can show also the conservation of momentum starting with the Newton's second law

$$\mathbf{F} = \frac{d\mathbf{p}_{mech}}{dt} \tag{2.15}$$

, then we write

$$\frac{d\mathbf{p}_{mech}}{dt} = \oint_{\partial V} \overleftrightarrow{\mathbf{T}} \cdot \mathbf{n} da - \frac{1}{4\pi c}\frac{d}{dt}\int_V (\mathbf{E} \times \mathbf{B}) dV \tag{2.16}$$

where $\mathbf{p}_{mech}$ is the mechanical momentum of the particles contained in volume V. The second term of the right-hand-side of the expression is the field momentum, which is the momentum carried by electromagnetic fields.

$$\mathbf{p}_{field} = \frac{1}{4\pi c}\int_V (\mathbf{E} \times \mathbf{B}) dV \tag{2.17}$$

Hence, total momentum which is the sum of the mechanical and field momentum can

be written as

$$\frac{d}{dt}[\mathbf{p}_{mech} + \mathbf{p}_{field}] = \oint_{\partial V} \overleftrightarrow{\mathbf{T}} \cdot \mathbf{n} da \tag{2.18}$$

For time-harmonic fields, the average of the field momentum term over one oscillation period vanishes. The remaining expression for the time-averaged force is

$$\langle \mathbf{F} \rangle = \oint_{\partial V} \langle \overleftrightarrow{\mathbf{T}} \rangle \cdot \mathbf{n} da \tag{2.19}$$

$\overleftrightarrow{\mathbf{T}}$ is actually the force per unit area acting on the surface, and the diagonal elements represent pressures and off-diagonal elements represent shears. Equation 2.20 allows one to calculate the mechanical force on a body within the closed surface. The force is determined by the electric and magnetic fields on the surface ∂V.

For macroscopic media, the field momentum density $\mathbf{g}$ and the Maxwell stress tensor is

$$\mathbf{g} = \frac{1}{4\pi c}(\mathbf{E} \times \mathbf{H}) \tag{2.20}$$

$$T_{ij} = \frac{1}{4\pi}[E_i D_j - \frac{1}{2}\delta_{ij}(\mathbf{E} \cdot \mathbf{D}) + H_i B_j - \frac{1}{2}\delta_{ij}(\mathbf{B} \cdot \mathbf{H})] \tag{2.21}$$

The medium is assumed to be linear, but it is not necessary to be isotropic in i-direction. There is no restriction in size (except few atoms sizes) and shape of the body, as to its dielectric properties. This method is widely applicable, such as for purely electric, purely magnetic or fully electromagnetic effects, and for traveling or evanescent wave fields.

Rayleigh particles, that are having dimensions much smaller than the incident wavelength, can be described by a dipole as a simple model. The time-averaged force for the Rayleigh particles in the dipole approximation is given in the Appendix 1.

Chapter 3

THE SURFACE PLASMON ENHANCED OPTICAL FORCE ON A NANOROD PAIR

In this chapter, we investigate the surface plasmon enhanced optical force on a sub-wavelength nanorod pair in the presence of a dielectric interlayer. We first describe the plasmons and the surface plasmons generally. We work on the characterization of the optical force with respect to the permittivity and the thickness of the dielectric interlayer.

3.1 Surface plasmons

The electrons of a metal oscillate in response to the applied electric field and their motion is damped by the collisions. The damped oscillation is given by

$$m\ddot{x} + m\gamma\dot{x} = -eE \tag{3.1}$$

where m is the mass of the electron and γ is the collision frequency, the time harmonic dependence $exp(-i\omega t)$ is assumed. The displaced electrons result in polarization. Then

$$D = \epsilon_0(1 - \frac{\omega_p^2}{\omega^2 + i\gamma\omega})E \tag{3.2}$$

$$\omega_p = \frac{ne^2}{\epsilon_0 m} \tag{3.3}$$

The frequency dependent, complex dielectric function of the free electron gas is given by

$$\epsilon(\omega) = 1 - \frac{\omega_p^2}{\omega^2 + i\gamma\omega} \tag{3.4}$$

In the case of negligible damping, for large frequencies close to plasma frequency, the dielectric function can be described simply by

$$\epsilon(\omega) = 1 - \frac{\omega_p^2}{\omega^2} \tag{3.5}$$

Instead of dielectric function of the material, refractive index can be used to describe the optical properties , the dielectric function can be derived by the relation $\tilde{n} = \sqrt{\epsilon}$. If the dielectric function related to the refractive index is complex, then $\tilde{n} = n + \imath k$ where n is the real part and k is the imaginary part (loss in the material) of the refractive index.

Surface plasmon polaritons are electromagnetic surface waves which propagate along a metal-dielectric interface and evanescently confined in perpendicular direction.[Fig 3.1] They result from the coupling between electromagnetic fields and col-

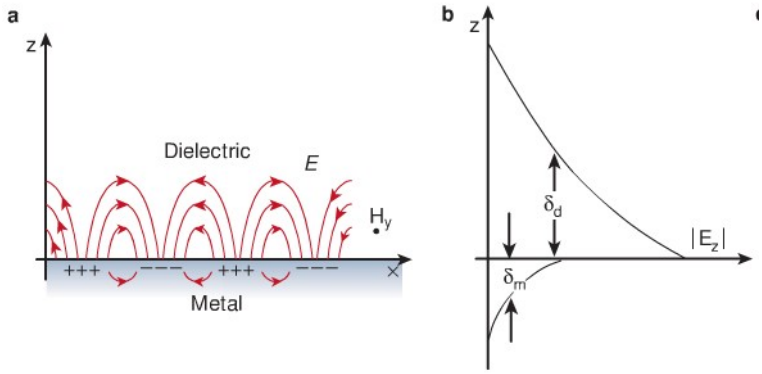

Figure 3.1: Surface plasmon propagating along the metal-dielectric interface and the evanescent decay of electric field perpendicular to the interface where δ_m is the skin depth of the metal and δ_d is the decay length of the field into the dielectric [37].

lective oscillations of the electron plasma of the conductor. Following the derivation given in [38], the surface plasmon polaritons at single interface can be excited only by the TM polarization. The dispersion relation of SPPs propagating at the interface is given by

$$\beta = k_0 \sqrt{\frac{\epsilon_1 \epsilon_2}{\epsilon_1 + \epsilon_2}} \tag{3.6}$$

where k_0 is free space propagation constant, ϵ_1 is the dielectric constant of the conductor and ϵ_2 is the dielectric constant of the dielectric medium. For large wave vectors, the frequency of the surface plasmon polaritons approaches the characteristic surface plasmon frequency, and can be found by inserting the dielectric function into the dispersion relation,

$$\omega_{sp} = \frac{\omega_p}{1 + \epsilon_2} \tag{3.7}$$

Figure3.2 shows the dispersion relation of SPPs at the interface of a metal with negligible damping and two possible media as air($\epsilon_2 = 1$) and silica($\epsilon_2 = 2.25$) On the contrary, in the case of subwavelength particles we encounter localized surface plasmons which are non-propagating excitations of electrons coupled to the electromagnetic field. When the particle size is much smaller than the wavelength of light, the quasi-static approximation is used to study localized surface plasmon on the particles in an harmonically oscillating electromagnetic field. The problem is treated as in an electrostatic field with an harmonic time dependence added to the solution. To achieve the surface plasmon resonance condition, the interaction between a metal nanoparticles and an electromagnetic wave is studied. So we are dealing with the solution of the Laplace equation, and then calculation of the electric field. We assume that a spherical particle is placed in an electric field having the field lines parallel

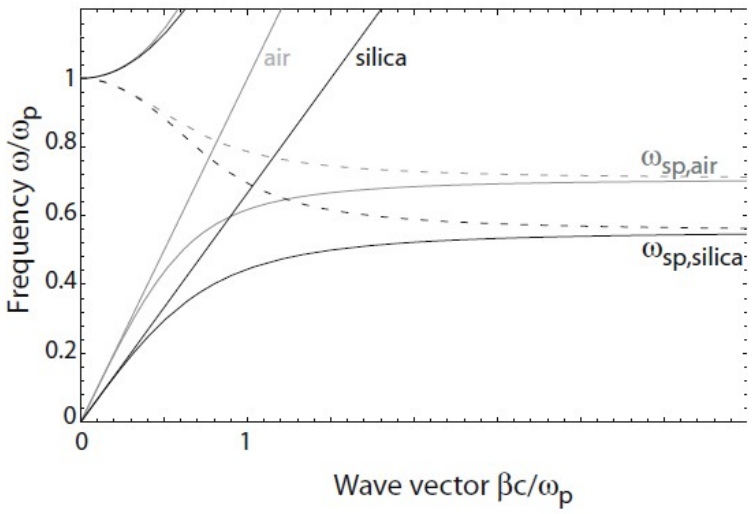

Figure 3.2: The dispersion relation of SPPs at the interface between metal and dielectric chosen to be air (gray curves) and silica (black curves). The real (continuous curves) and the imaginary part (broken curves) of the wave vector β is plotted [38].

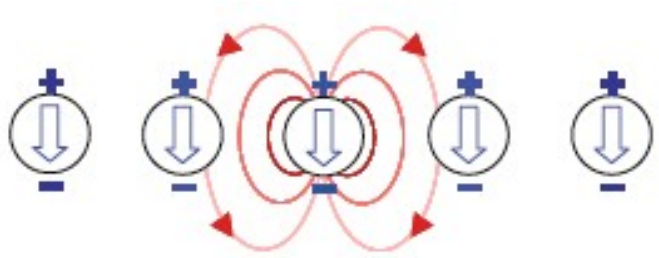

Figure 3.3: Near-field coupling between metallic nanoparticles [38]

to the z-direction. Following the solution from section 4.4 of [1], applying boundary conditions, the potentials inside and outside the sphere is

$$\Phi_{in} = \frac{-3\epsilon_m}{\epsilon + 2\epsilon_m} E_0 r cos(\theta) \tag{3.8}$$

$$\Phi_{out} = -E_0 r cos(\theta) + \frac{\epsilon - \epsilon_m}{\epsilon + 2\epsilon_m} E_0 a^3 \frac{cos(\theta)}{r^2} \tag{3.9}$$

where a is the radius of the sphere, ϵ is the dielectric function of the sphere and ϵ_m is the dielectric constant of the surrounding medium. Φ_{out} is the sum of the applied

field and that of a dipole located at the particle center. Introducing the polarizability α of the sphere in which a dipole moment p is induced by the electric field

$$p = \epsilon_0 \epsilon_m \alpha E_0 \tag{3.10}$$

$$\alpha = 4\pi a^3 \frac{\epsilon - \epsilon_m}{\epsilon + 2\epsilon_m} \tag{3.11}$$

we lead the resonance condition which is known as the Fröhlich condition. It is achieved when the real part of the frequency dependent dielectric function of the metal particle is equal to negative of two times the dielectric constant of the nonabsorbing surrounding medium

$$Re[\epsilon(\omega)] = -2\epsilon_m \tag{3.12}$$

Here the factor (2) for the resonance condition is for the spherical particles. However, it can be generalized defining the geometrical factor for differently shaped particles like ellipsoids, cylinders. The polarizability shows a resonant enhancement when its denominator is a minimum, so for the small or slowly-varying imaginary part of the dielectric function around the resonance, we can take only the real part of the dielectric function and then the Fröhlich condition is obtained. A consequence of the resonance is the enhancement of the fields. For gold and silver nanoparticles, the resonances are at the visible wavelengths.

The localized plasmon resonance frequency of the metallic nanoparticle can be shifted depending on size and shape of the nanoparticle as well as the physical environment as discussed in ref [39]. In [38], we see that the extinction cross section calculation for a silver sphere immersed in two different media displays two different single peaks respective to each medium. The scattering spectra is given for different shapes showing shifted peaks at their plasmon resonance frequencies. As all these

discussions summarized in reference [40], the coupling between the nanoparticles is responsible for changing the spectrum. The near field produced by the dipole excited in the nanoparticle is effecting the closely spaced another nanoparticle(Fig 3.3). This coupling between the nanoparticles is the cause of the shift in resonance frequency. For these small particles, the interaction is of a dipolar nature. Furthermore, depending on the polarization of the illuminating wave, the plasmon resonance can be blue or red shifted. Other than the explanation given by dipolar interaction, the hybridization model has been applied to nanoparticle dimers to calculate the resonance frequency [41].

3.2 Computational procedure

We employ Comsol Multiphysics, which is a finite element method, to solve the scattering problem of the subwavelength metallic particle illuminated by a plane wave.

We perform a 3D simulation. The geometry is constructed for the vacuum case. The nanostructure's center of mass is placed at the origin of a large spherical computational domain where the most outer layer is chosen to be Perfectly Matched Layer (PML). PML is a layer absorbing the incident radiation on it without creating reflections from the boundary. It is absorbing radiation coming from wide range of incidence angles. The size of the computational domain is set to be equal to one half of the excitation wavelength, so that the computational size is adjusted with respect to the excitation wavelength in order to reduce memory and execution time.

For reducing the computational memory, the mesh is defined differently on the domains with different sizes and materials. The maximum mesh size for the domains except the nanostructures, are one sixth of the wavelength. For the nanostructures, a much refined mesh is selected. Also, we are more careful for mesh distribution to be symmetric around the nanorods, because the Maxwell stress tensor integration

around the nanorods are very sensitive to mesh.

The THz frequencies corresponding to a wavelength range 600-800 nm are studied. We employ a parametric sweep node under the frequency domain study. The incident plane wave is given as an input for the background electric field under the "electromagnetic waves" node which solves for the scattered field. The electric field polarized along the z-axis is given as $E_0 exp(-jk_0 x)$, where k_0 is the vacuum wave vector.

The gold permittivity values are taken from the Johnson and Christy [42] and interpolated to construct a frequency dependent dielectric function in the relevant frequency range.

The dimensions of the dielectric interlayer in the next step are carefully chosen. A touching dielectric slab with the nanorods causes some numerical problems about the boundary and domain definitions.

The optical force calculation are done on the surface defined as a cylinder with hemispherical caps encapsulating each nanorod separately. Theoretically, any integration surface should work, such as a simple rectangular box. However we experienced numerical difficulties due to the discontinuities at the box edges, hence a smooth surface is better for numerical purposes. The force calculation can be done directly on the nanorod. However as mentioned in ref. [43], we need an integration surface where all fields are well-defined. We verify this requirement by calculating the force components on the surface of the nanorod, we see that the all forces are exactly equal to zero. Moreover, the integration surface encapsulating a single nanorod is restricted not to intersect with any other boundary such as the dielectric interlayer or the other nanorod. Again the mesh is carefully designed between the nanorod surface and the integration surface.

A typical simulation is based on a discrete mesh with approximately $9x10^5$ nodes. The total computation time for 40 frequency values through a parametric sweep

requires approximately 40 minutes on a PC (Intel Core i7 processor and 8 GB system memory). In order to reduce the time and memory requirements, it is possible to use symmetry planes, however the calculated force results were not matching the expected ones in our construction. Hence we employed a full 3D computation.

3.3 Optical force on a gold nanorod pair in vacuum

We begin by calculating a reference force spectrum for the gold nanorods in vacuum. Figure 3.4 shows the geometrical parameters of the nanorod pair with an inter-rod dielectric layer. The diameter of the nanorods is $D = 25$ nm, length is $L = 100$ nm, distance between the nearest sides of nanorods is $d = 35$ nm. A plane wave polarized along the long z-axis of the nanorods is propagating along the x-direction as shown in the figure. We label the nanorod to which the electromagnetic wave is incident, as "2" and the other nanorod as "1". The common force is defined as ($F_{common} = (F_1 + F_2)$)

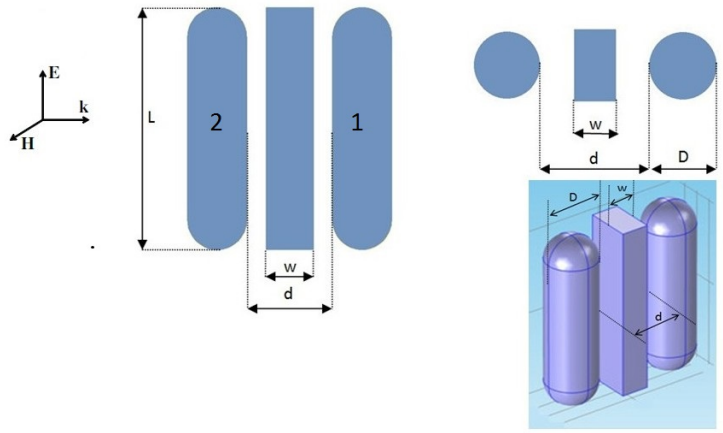

Figure 3.4: The geometrical parameters of the two gold nanorods with an inter-rod dieletric layer, which can be taken as air to model the vacuum case,are denoted. The side, top, and isometric view of the model is plotted. The polarization and the propagation direction of the incident em radiation is shown.

which is acting on the center of mass .The relative force between nanorods is defined as ($F_{relative} = (F_1 - F_2)/2$). According to this definition, a negative relative force

tends to decrease the distance between the nanorods, hence it is attractive, whereas a positive relative force between the nanorods implies a repulsive behavior. The relative force exhibits two resonance, one of which corresponds to the resonance of the electric dipole moment and the other corresponds to the resonance of the magnetic dipole moment. The electric dipole moment is calculated using

$$p_z = \iiint_V P_z dV = \iiint_V (D_z - \varepsilon_0 E_z) dV \tag{3.13}$$

where P_z is the z-component of the polarization and D_z is the z-component of the displacement field. The magnetic moment is calculated from $\mathbf{r} \times \mathbf{J_p}$ (r is the position vector pointing the volume element that contains the current density) , which yields

$$m_y = \iiint_V (z\frac{\partial P_x}{\partial t} - x\frac{\partial P_z}{\partial t}) dV \tag{3.14}$$

$$= -i\omega \iiint_V [z(D_x - \varepsilon_0 E_x) - x(D_z - \varepsilon_0 E_z)] dV \tag{3.15}$$

where ω is the frequency of the time harmonic fields. We also include the common and relative forces for a perfect electric conductor (PEC) in Fig. 3.6 which does not display any resonance and smaller in magnitude with respect to the force spectra of the two gold nanorods.

At 422 THz, the magnetic dipole moment has a maximum as antisymmetric eigenmode leading to an attractive Coulomb force, since the antisymmetric mode causes a charge distribution such that the charges with opposite sign accumulates at the same end of each nanorod Fig. 3.5 a. At 445 THz, the electric dipole moment has a maximum as symmetric mode leading a repulsive force (Fig. 3.6). We studied also optical forces for different interwire distances. The magnitude of the peak increases for smaller inter-rod distance, and the resonance peaks shifts towards the higher frequencies.

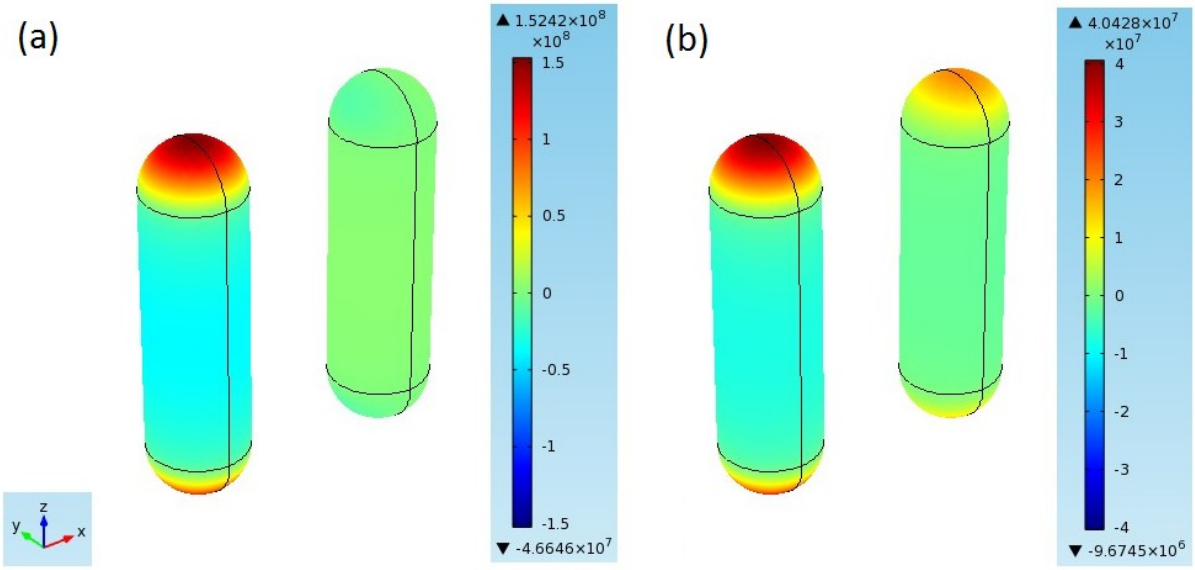

Figure 3.5: (a)The E_z is plotted at magnetic dipole resonance (422 THz) corresponding to an attractive force. (b) The E_z is plotted at the electric dipole resonance (445 THz) resulting in a repulsive force.

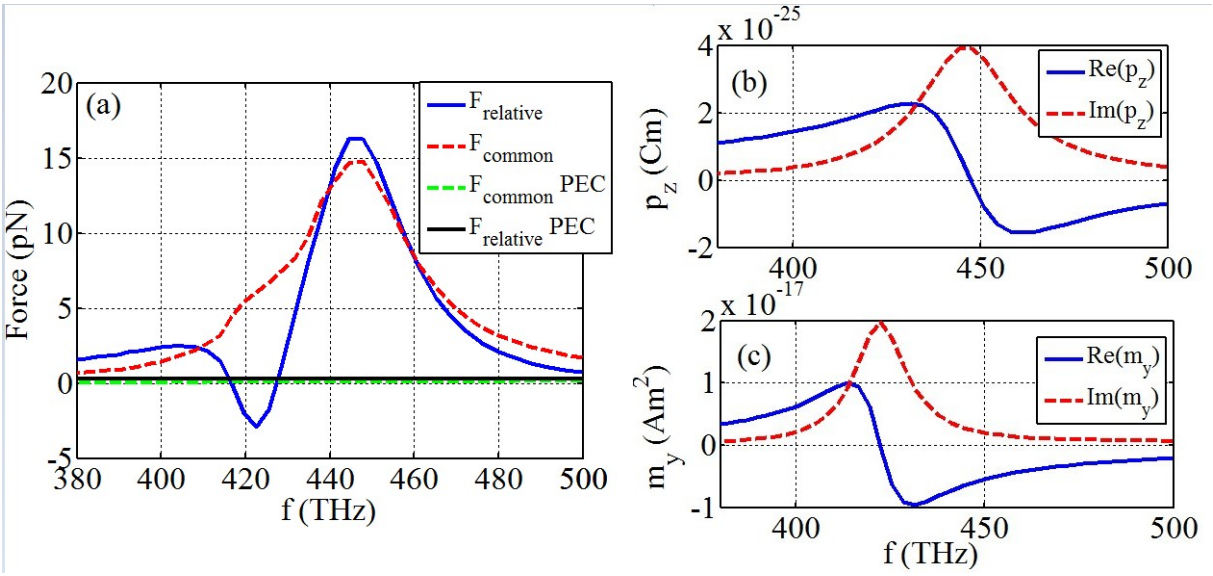

Figure 3.6: (a) The frequency spectra of the relative (solid blue curve) and common (dashed red cuve) force in the nanorod pair system. The nanorods are of length 100 nm, diameter 25 nm and interwire distance 35nm. The common (green dashed) and relative (solid black curve) force for PEC. (b-c) The real (solid blue curve) and imaginary (dashed red curve) parts of the (b) electric and (c) magnetic dipole moment of the nanorod pair.

3.4 Optical force on gold nanorods with a dielectric interlayer slab

We introduce a dielectric interlayer between the nanorods and we investigate its effect on the optical force. For this system, all the geometrical parameters of the reference system (i.e. rod pair in vacuum) are kept fixed. The inserted dielectric slab has length 100 nm, depth 25 nm, and thickness w which varies from 15 nm to 30 nm. Another parameter for the characterization of the optical force is the dielectric constant ϵ of the inter-rod slab. We assume that the dispersion of the dielectric material is constant and the dissipation is negligible, which may be justified for a nanometer thick dielectric layer subject to THz frequency fields. If the dielectric material is not highly lossy, dissipation would not have a significant effect. The dispersion of the dielectric materials is smooth in THz frequencies. The common and relative forces are calculated in the same way defined in previous section.

In the first part of our analysis, we keep the dielectric constant of the interlayer constant at $\epsilon = 3$, and study the system for different interlayer thicknesses. We plot the individual calculated forces on each of the nanorods(Fig 3.7). The figure shows that the peak position of the force F_1 is redshifted as the thickness of the dielectric slab increases. Like F_1 peak values, the F_2 resonances are redshifted, but the interesting point is that the electric dipole associated peak exceeds the F_1 increasing the dielectric interlayer thickness w. As a result, in the relative force graph we observe the sign change (Fig 3.8). The results show that filling more space between nanorods with dielectric material, the resonances are both magnified and red shifted. The shift is greater for the peak corresponding to magnetic resonance.

In the second part of the analysis, we study the optical forces when the thickness of the slab is kept constant at $w = 25$ nmand the dielectric constant ϵ is varied. We plot the individual force spectra in Fig. 3.9, and the common and relative forces in Fig. 3.10. Again the peak in the F_2 corresponding to electric dipole resonance

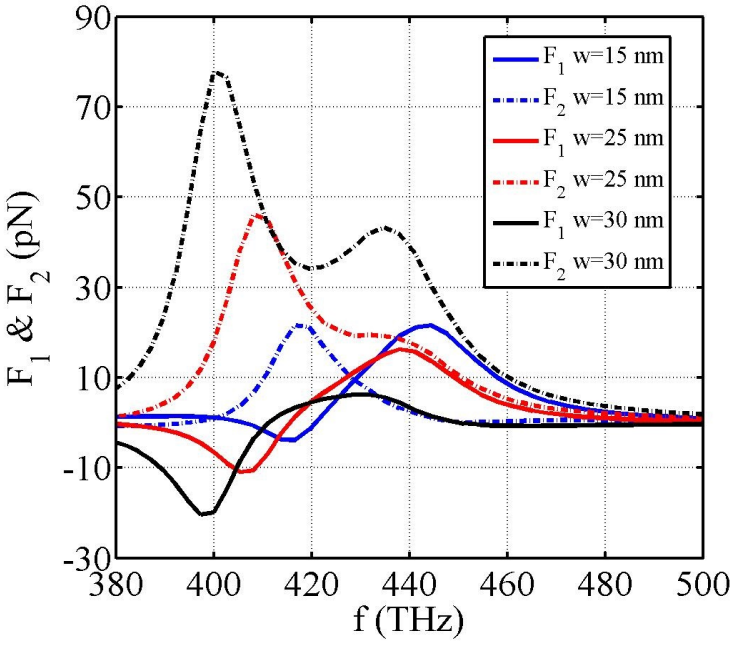

Figure 3.7: calculated individual force (F_1 solid curves,F_2 dashed curves) spectra of nanorods in the presence of a dielectric interlayer for fixed $\epsilon = 3$ $w = 15, 25, 30$ nm.

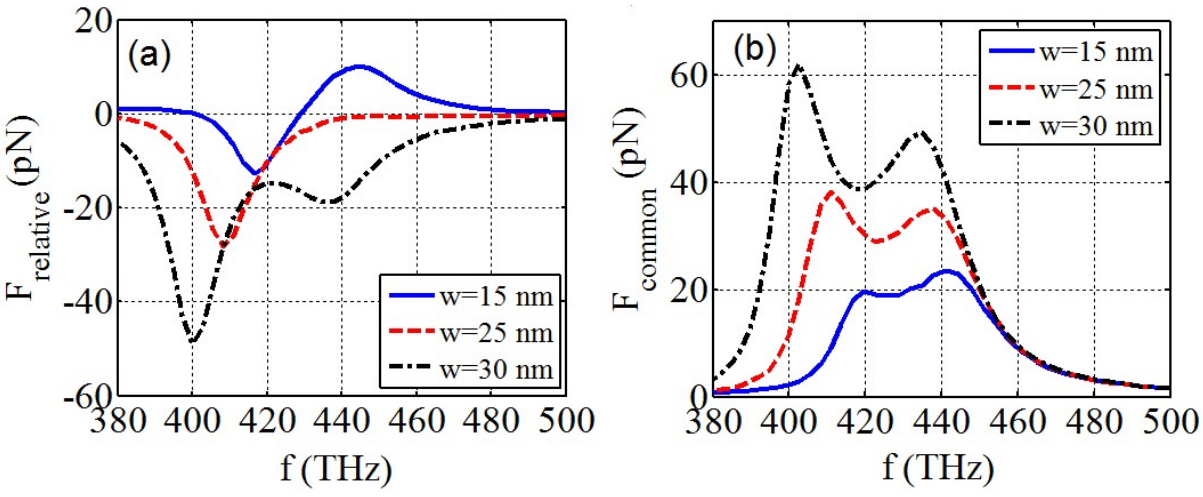

Figure 3.8: The (a) relative and (b) common force spectra of nanorod pair with a dielectric interlayer of different thicknesses and of a constant permittivity $\epsilon = 3$.

experiences a sign change from negative to positive with increasing permittivity of the dielectric slab,which in turn leads to reversal of the relative force at 440 THz.

The relative force peak values are at 422 THz and 445 THz for $\epsilon = 1$, at 408 THz

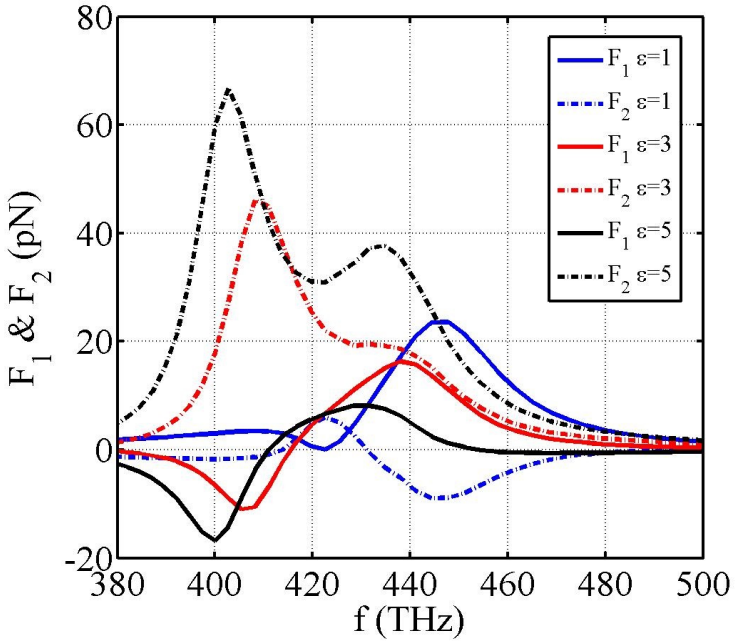

Figure 3.9: The calculated individual force spectra of nanorods in the presence of a dielectric interlayer for fixed $w = 25$ nm, $\epsilon = 1, 3, 5$.

and 441 THz for $\epsilon = 3$, and at 402 THz and 436 THz for $\epsilon = 5$. In Figures 3.11 (a)

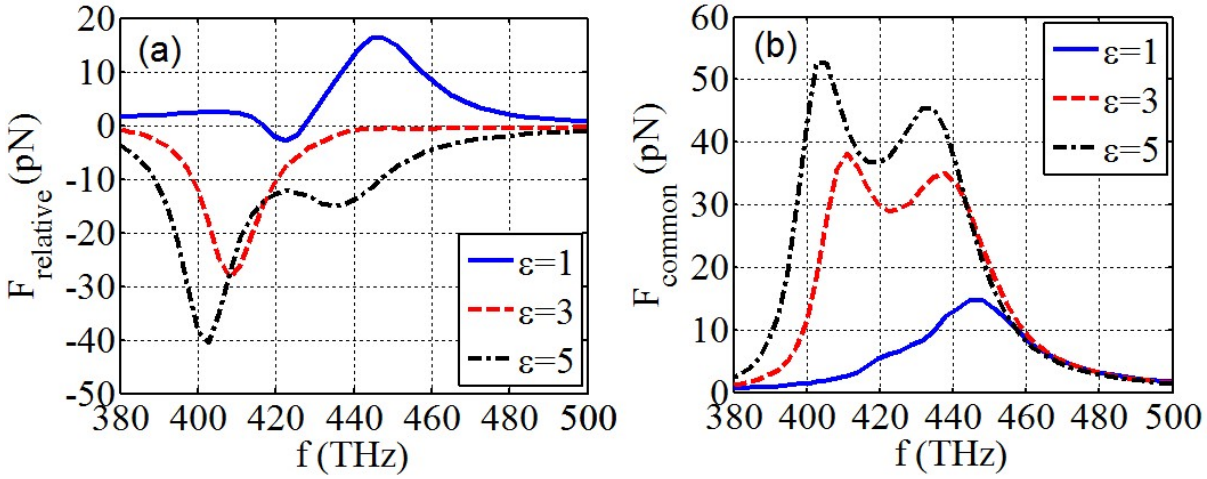

Figure 3.10: The (a) relative and (b) common force spectra of nanorod pair with a dielectric interlayer of different permittivities and of a constant thickness $w = 25$ nm.

and (b), we plot the force at two selected frequencies as a function of the permittivity with fixed thickness ($w = 25$ nm) and as a function of the thickness with fixed permittivity ($\epsilon = 3$), respectively. In Figure 3.11 (a), the relative force as a function of dielectric constant is all attractive for 427 THz (dashed lower curve), whereas it exhibits a sign change for 445 THz and it crosses the zero approximately at $\epsilon = 3$ (solid lower curve). The common force at 427 THz (upper dashed curve) is increasing monotonically with increasing permittivity. The common force at 445 THz (upper solid curve) increases up to $\epsilon = 3$, and decreases afterwards. In Figure 3.11 (b), the relative force with respect to thickness of the interlayer decreases monotonically and reverses sign at $w = 24.5$ nm for 445 THz (lower solid curve). The relative force at 427 THz (lower dashed curve) is attractive throughout the range. The common force at both frequencies (upper two curves) increases with increasing thickness.

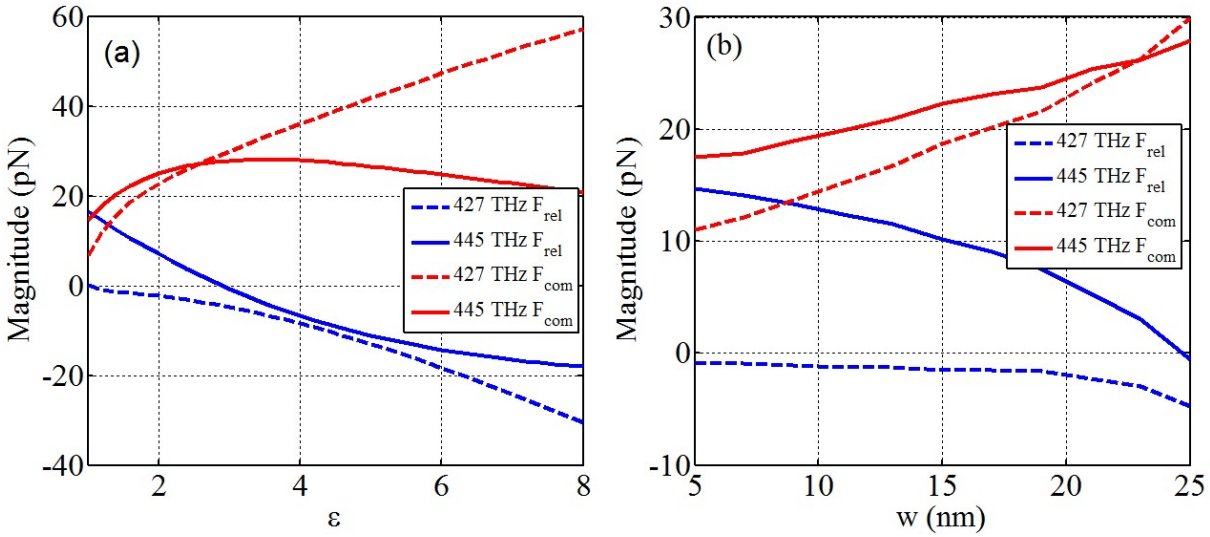

Figure 3.11: The common- (upper two curves) and the relative force (lower two curves) as a function of permittivity for a 25 nm thick dielectric interlayer at 427 THz (dotted) and 445 THz (solid); (b) Same as in (a) but as a function of thickness of a dielectric interlayer of $\epsilon = 3$.

We can conclude that increasing the electromagnetic field energy between the rods either by increasing the permittivity or the volume of the dielectric material occupying

the space between the nanorods enhances the common force which is always repulsive. The direction of the relative force may not be explained solely from the symmetry of the excitation mode of the nanorods as it was in the absence of the dielectric layer. The polarization of the dielectric layer contribute to the local field distribution at the nanorod surfaces where the optical forces are calculated. The relative force at the magnetic dipole resonance remains attractive and increases in magnitude, whereas the relative force at the electric dipole resonance changes sign from positive to negative.

3.5 Tunable relative force by the use of liquid crystals

These results suggest that a tunable optical force may be achieved by incorporating a dielectric material whose refractive index can be controlled externally. Here, we propose the use of a birefringent liquid crystal. Birefringent liquid crystals exhibit ordinary and extraordinary refractive indices determined by the polarization of the incident radiation (perpendicular or parallel respectively) to the director. In the presence of an external field, the re-orientation of the director axis occurs. Therefore applying voltage externally to the slab, the change in refractive index can be achieved. If we place a liquid crystal with its director along the x-direction, and then applying voltage in z-direction we can align the director parallel to the polarization of the incident em wave. In Figure 3.12, we plot the optical forces obtained in the presence of a liquid crystal interlayer of thickness $w = 25$ nm. The refractive index data of the liquid crystal is taken from Ref. [44]. As shown in Fig. 3.12 (c), it is possible tune the relative optical forces in an attractive/repulsive regime at a frequency of 440 THz.

In this chapter, we studied the optical force provided by an incident plane wave on the nanorod pair and the effect of a dielectric interlayer on the optical forces. The relative optical force exhibits both repulsive and attractive behavior due to asymmetric placement of the nanostructure with respect to the propagation of the electromag-

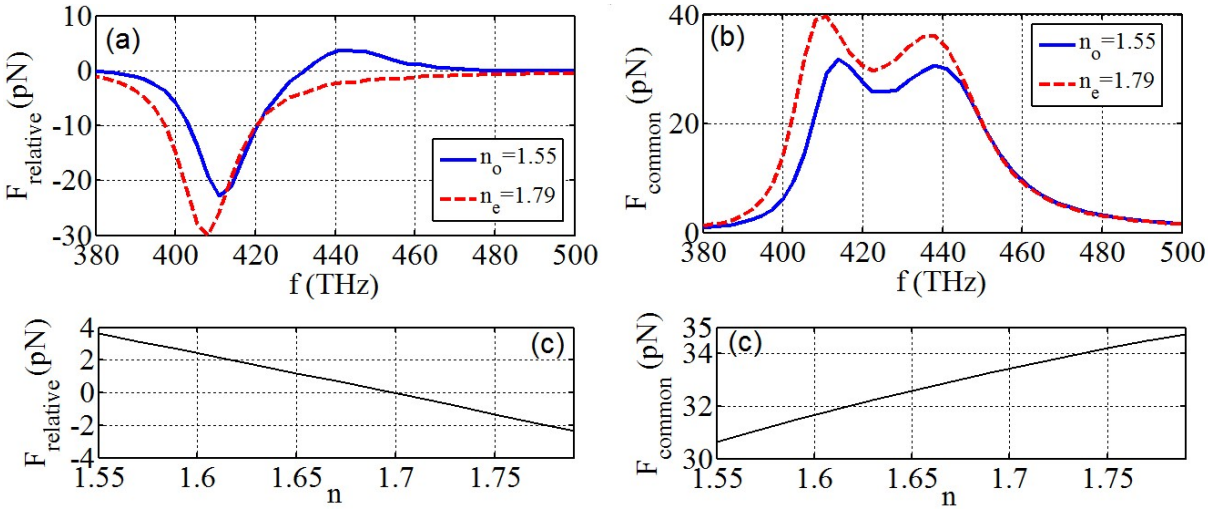

Figure 3.12: The (a) relative and (b) common force spectra with a liquid crystal interlayer of thickness $w = 25$ nm with the two extreme values of its refractive index from 1.55 to 1.79 under the voltage effect. (c) The relative (blue solid) and common force (red dotted) plotted as a function of refractive index at 440 THz.

netic radiation. In the next chapter, we will investigate the optical force between coupled dielectric waveguides, however in this case the optical force exerted on each waveguide is due to the gradient forces.

Chapter 4

OPTOMECHANICAL FORCES BETWEEN COUPLED WAVEGUIDES

In this chapter, I present two coupled dielectric waveguides and the simulation results for mode solutions of the coupled system. For two eigenmodes of the system, we calculate optical forces on the waveguides. In the last part of this chapter, the deformation of the waveguides due to the optical force is studied.

The modes of the coupled system can be explained by the coupled mode theory given in Appendix 2. The eigenvalues of the system are the symmetric and anti-symmetric propagation constants β_s and β_a in terms of the individual propagation constants of the waveguides and the coupling coefficient.

In our study, we should note that we directly excite the coupled modes (symmetric and antisymmetric mode) and we do not expect any power transfer along the propagation which is given by

$$L_c = \frac{\pi}{\beta_s - \beta_a} \tag{4.1}$$

We will investigate the power transfer between the waveguides for the metal dielectric strip waveguides system.

4.1 Optical force between coupled waveguides

In this section, we study the optical forces between two coupled linear dielectric waveguides. This system was studied by Povinelli and her group in 2005 [14]. The

evanescent tails of the guided modes of the waveguides overlap and result in either attractive or repulsive optical force. The model consist of two parallel, silicon (refractive index 3.45) waveguides which are separated by a distance d. Each waveguide has a square cross section having side dimension $a = 310$ nm (Fig 4.1).The wavelength is 1550nm.

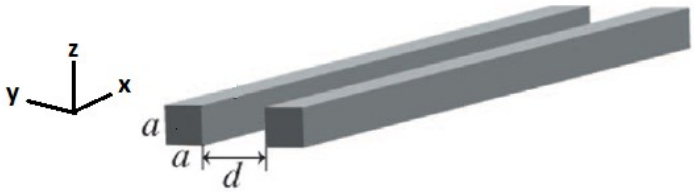

Figure 4.1: Two rectangular silicon waveguides of side length a is plotted. The distance between them is d.

For infinite separation between the waveguides, no coupling occurs. Modes of the two isolated waveguides are degenerate; as the waveguides come closer, the degeneracy is broken, and two distinct eigenmodes appear. We first consider two-dimensional waveguides (translational invariance along the propagation direction) and then investigate the three-dimensional coupled waveguide system.

For 2D simulation, we construct the geometry, that is only the rectangular cross section of the waveguides. We set the material properties of the waveguides as silicon and the surrounding domain as air. After meshing the computational domain, we decide the desired number of the modes under the mode analysis node of the software. We get the possible eigenmodes of the coupled waveguides system and the corresponding the effective indices. The resulting field profiles for the symmetric and antisymmetric modes are plotted on the cross section of the waveguides where the ratio $r = d/a = 0.6$ in the Fig. 4.2. The y-component of the force, as a function of the ratio r with fixed parameter a, is plotted in Fig. 4.3. The two coupled modes lead to either attractive or repulsive force on each other depending on the distance between

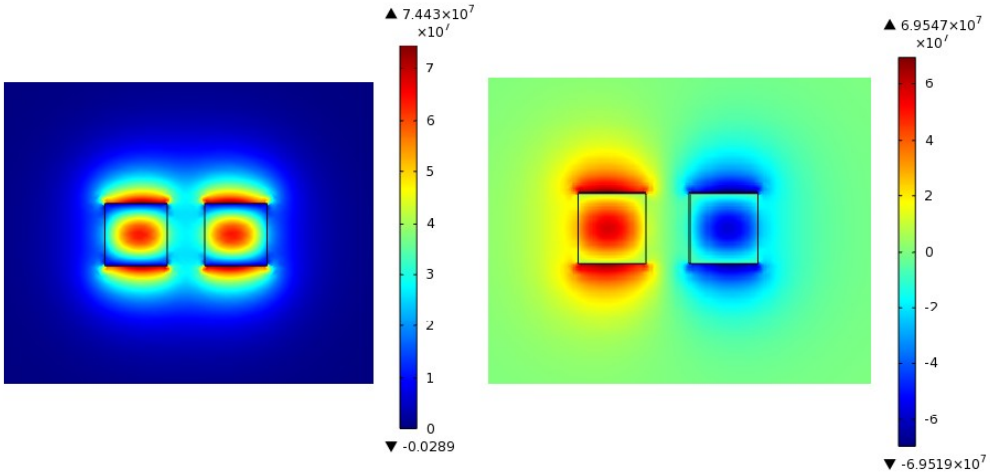

Figure 4.2: Ez field is plotted for symmetric and antisymmetric modes.

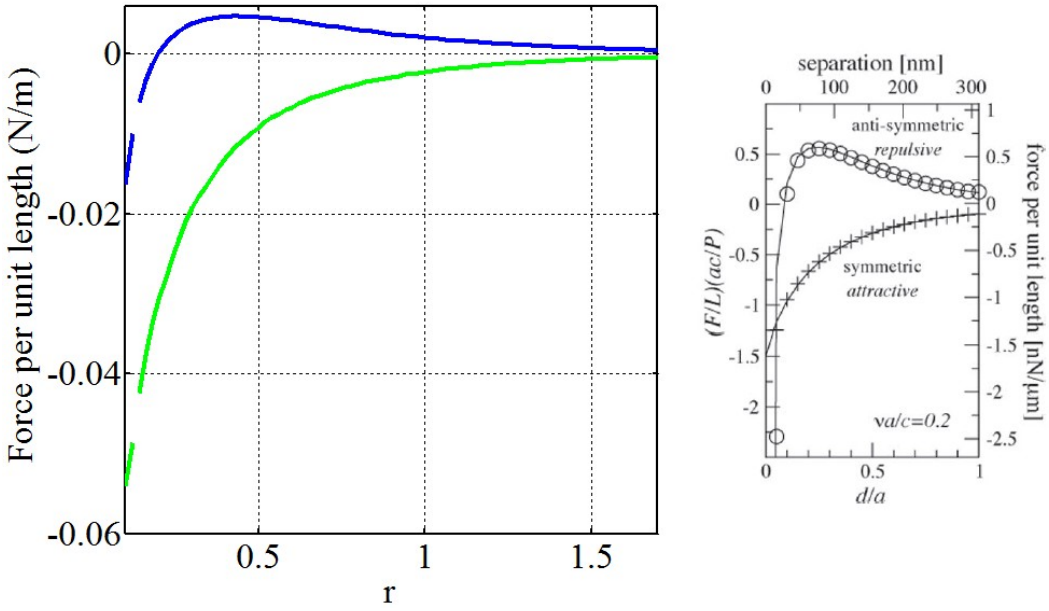

Figure 4.3: Force per unit length is calculated integrating Maxwell stress tensor on the surface of the waveguide as a function of the ratio r for symmetric (green) and antisymmetric (blue) modes. The comparison with the force calculation from Ref. [14].

the waveguides. The antisymmetric mode results in an attractive force for $r/a < 0.2$ separation. For larger separations, the force is repulsive and it has maximum value for the ratio $r = 0.4$, and it decays to zero. For the symmetric mode, the force is

negative for all rs (i.e. separations) and similarly it approaches to zero where the degeneracy broken due to coupling is reconstituted.

In reference [14], it is demonstrated that the mechanical force can be calculated using the following expression. It is assumed that energy $U = N\hbar\omega$ is coupled into an eigenmode with frequency ω and wavevector k of the system of two waveguides separated by a distance ξ. An adiabatic change in separation $\Delta\xi$ will shift the eigenmode frequency by $\Delta\omega$. Then the force is given by

$$F = -\frac{dU}{d\xi}\Big|_k = -\frac{d(N\hbar\omega)}{d\xi}\Big|_k \tag{4.2}$$

$$= -N\hbar\frac{d\omega}{d\xi}\Big|_k = -\frac{1}{\omega}\frac{d\omega}{d\xi}\Big|_k U \tag{4.3}$$

The full derivation leading to Eq.s 4.16 and 4.17 can be found in Ref. [30]. However, we stress that this method is not accurate in plasmonic systems as discussed in [33].

Our ongoing research is on the coupled metal dielectric strip waveguides. The gold (Au) strip has width 8 μm and heigth 12 nm, the silicon-nitride (SiN) waveguide has width 6 μm and heigth 32 nm (Fig. 4.4). As shown in Ref. [47], for TM polarization, the coupling occurs when the metal strip can support the long range surface plasmon polariton (LRSPP) waveguide mode. We directly excite the eigensolution of the coupled waveguides and we determine the modes of the coupled system (Fig. 4.5). Next, we will solve the problem of the power coupling between the waveguides and we will study the optical forces between plasmonic metal strip and dielectric waveguide.

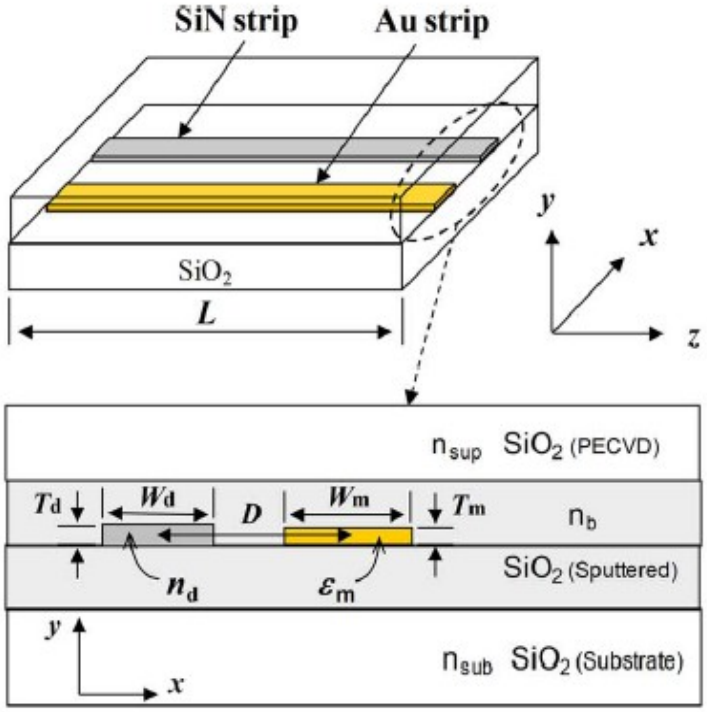

Figure 4.4: Schematic structure of the hybrid coupler with Au strip (yellow) and SiN strip (gray) surrounded by silica. The refractive indices are $n_d = 1.871$, $n_{sup} = 1.448$, $n_b = 1.453$ and $n_{sub} = 1.446$ [47].

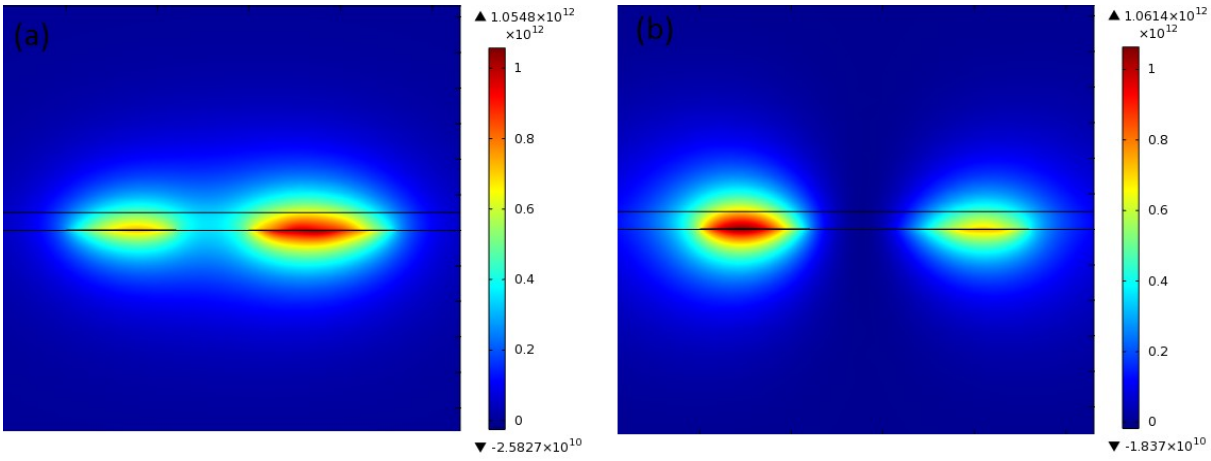

Figure 4.5: The two eigenmodes (symmetric (a) and antisymmetric (b) profiles) of the coupled Au-SiN waveguide system is shown. The power flow along the propagation direction is plotted.

4.2 Mechanical deformation effects

The optomechanical results are studied using structural mechanics module of Comsol Multiphysics. The (elasticity) poisson ratio and young modulus of the material forming waveguides are taken as 0.22 and 169[GPa] respectively. The attractive optical force resulted from coupled symmetric mode of the waveguides is provided as a load on the waveguide structure in air which is clamped at both ends. The displacement of ends of the waveguides are zero taking the ends fix. We take $d/a = 0.15$, and the length of the waveguides set to be $30\mu m$. The force load per unit length is 0.7nN/um read from the force spectrum for given ratio r. Under static equilibrium, the waveguides are bent. The plot depicts the bend in comparison to the straight position of the waveguides (Fig 4.6). . For a load of 0.7 nN/μm, the displacement at the midpoint

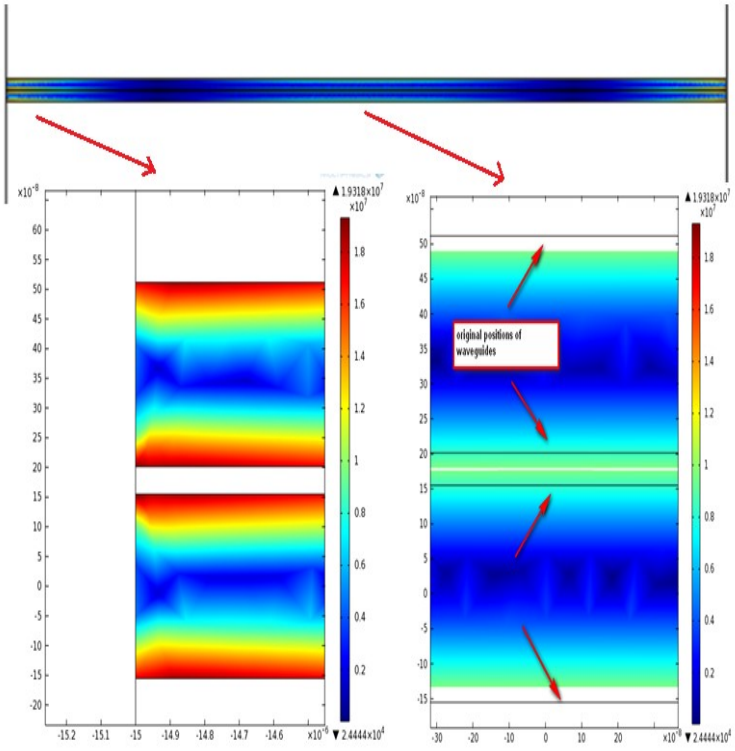

Figure 4.6: At a distance of 46.5 nm, the attractive force result in bend waveguides toward each other.

of the waveguides is about 21 nm.

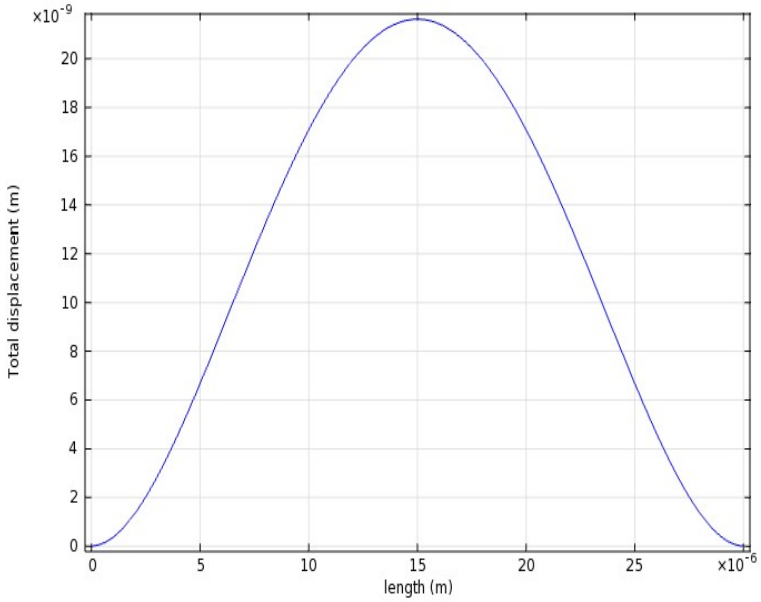

Figure 4.7: The total displacement experienced by the waveguide along the propagation direction when the attractive force of 0.7nN/μm is applied.

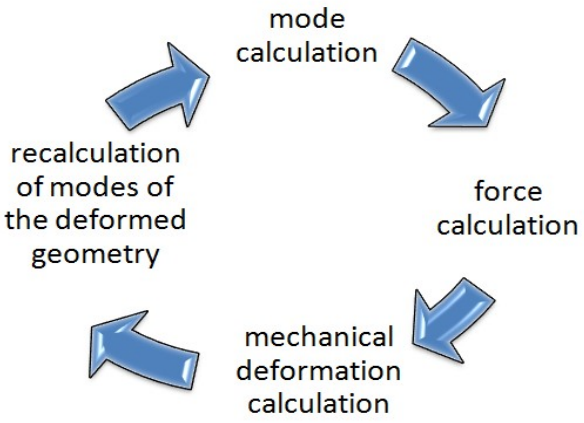

Figure 4.8: The schema of the self-consistent calculation.

The significant displacement from the axial direction of the waveguide may in turn affect the propagating modes since the coupling between the waveguides would change along the axis. Here we outline a self-consistent procedure that we will be working on in the future. The procedure that we want to follow is depicted in Fig. 4.8. We start by solving the modes of the coupled waveguides employing the mode analysis module. Using the solution data, we calculate the optical force by integrating the Maxwell stress tensor on the surface of the waveguide. Then, we apply the resulting force and obtain the deformed waveguides. Next, we recalculate the modes propagating in the deformed waveguides system. At present, we are working on implementing the self consistent calculation between the electrodynamics and structural mechanics modules.

Chapter 5

CONCLUSION

In this thesis, we have investigated the optical forces in two separate systems: (i) The surface-plasmon enhanced optical forces in illuminated coupled metallic nanorod pairs and (ii) the optical forces arising from coupled modes of dielectric waveguide pairs. Here, we summarize our major results and conclusions. For metallic nanorod pairs with a dielectric interlayer, we have found that the optical forces generated by an external electromagnetic plane wave depend on the permittivity or the thickness of the dielectric interlayer. In particular, when the optical forces acting on individual nanorods are combined as common and relative force components of the nanorod pair, we found that the relative force can be altered to become attractive or repulsive. This reversal in the relative force can be utilized as a tunable optical force in plasmonic nanostructures employing liquid crystals. The common force is always repulsive and its magnitude gets enhanced with increasing the permittivity or the thickness of the dielectric interlayer.

For two planar dielectric waveguides coupled by their evanescent waves, we have obtained optical forces according to mode solutions. The optical force is attractive and repulsive for symmetric and antisymmetric modes respectively. As a result of an attractive force, the structural mechanics simulation showed that the waveguides which are extending in air with fixed ends deform towards each other.

Optical forces can be explored in other configurations of nanorod pair such as periodic array of nanorods. We are investigating that the optical forces can affect the mode profile significantly due to the non-uniform coupling distance between the

deformed waveguides. Furthermore, we are investigating the effect of the surface plasmons on optical forces between a metal strip waveguide coupled to a dielectric waveguide.

BIBLIOGRAPHY

[1] Jackson, *Classical Electrodynamics, 2nd edition* (John Wiley Sons).

[2] $http://www.nasa.gov/missionpages/tdm/solarsail/solarsailoverview.html$.

[3] Favero, I. and Karrai, K., *Optomechanics of deformable optical cavities* Nature Photonics, vol. 3, 2009.

[4] Ashkin, A., *Acceleration and trapping of particles by radiation pressure* Phys.Rev.Lett., vol. 24, 1970.

[5] Ashkin, A., Dziedzic, J.M., Bjorkholm, J.E. and Chu,S., *Acceleration and trapping of particles by radiation pressure* Optics Letters, vol. 11, 1986.

[6] Chaumet, P.C. and Nieto-Vesperinas, M., *Time-averaged total force on a dipolar sphere in an electromagnetic field* Optics Letters, vol. 25, 2000.

[7] Arias-Gonzalez, J.R. and Nieto-Vesperinas, M., *Optical forces on small particles: attractive and repulsive nature and plasmon-resonance conditions* JOSA A, vol. 20, 2003.

[8] Halterman, K., Elson, J.M. and Singh, S., *Plasmonic resonances and electromagnetic forces between coupled silver nanorods* Phys.Rev.B, vol. 72, 2005.

[9] Zelenina, A.S., Quidant, R. and Nieto-Vesperinas, M., *Enhanced optical forces between coupled resonant metal nanoparticles* Optics Letters, vol. 32, 2007.

[10] Hallock, A.J., Redmond, P.L. and Brus, L.E., *Optical forces between metallic particles* PNAS, vol. 102, 2005.

[11] Liu, H., Ng, J., Wang, S.B., Hang, Z.H., Chan, C.T. and Zhu, S.N., *Strong plasmon coupling between two gold nanospheres on a gold slab* New Journal of Physics, vol. 13, 2011.

[12] Zhang, Q., Xiao, J., Zhang, X.M. and Yao, Y., *Optical binding force of gold nanorod dimers coupled to a metallic slab* Optic Communications, vol.301, 2013.

[13] Li, M., Pernice, H.P. and Tang, H.X., *Tunable bipolar optical interactions between guided lightwave* Nature Photon, vol. 3, 2000.

[14] Povinelli, M.L., Loncar, M., Ibanescu, M., Smythe, E.J., Johnson, S.G., Capasso, F. and Joannopoulos, J.D., *Evanescent-wave bonding between optical waveguides* Optics Letters, vol. 30, 2005.

[15] Yang, X., Liu, Y., Oulton, R.F., Yin, X. and Zhang, X., *Optical forces in hybrid plasmonic waveguides* Nano Letters, vol. 11, 2011. Huang, C. and Zhu, L., *Enhanced optical forces in 2D hybrid and plasmonic waveguides* Optics Letters, vol. 35, 2010.

[16] Chen, L., Zhang, T., Li ,X. and Huang, W., *Novel hybrid plasmonic waveguide consisting of two identical dielectric nanowires symmetrically placed on each side of a thin metal film* Optics Express, vol. 20, 2012.

[17] Li, H., Noh, J.W., Chen, Y. and Li, M., *Enhanced optical forces in integrated hybrid plasmonic waveguides* Optics Express, vol. 21, 2013.

[18] Zhang, J., MacDonald, K.F. and Zheludev, N.I., *Optical gecko toe: Optically controlled attractive near-field forces between plasmonic metamaterials and dielectric or metal surfaces* 2012.

[19] Ginis, V., Tassin, P., Soukoulis, C. and Veretennicoff, I., *Enhancing optical gradient forces with metamaterials* Phys.Rev.Lett., vol. 110, 2013.

[20] Thourhout, D.V. and Roels, J., *Optomechanical device actuation through the optical gradient force* Nature Photonics, vol. 4, 2010.

[21] Li, M., Pernice, W.H.P., Xiong, C., Baehr-Jones, T., Hochberg, M. and Tang, H. X., *Harnessing optical forces in integrated photonic circuits* Nature, vol. 456, 2008.

[22] Svoboda, K. and Block, S.M., *Biological Applications of Optical Forces* Annurev., 1994.

[23] Simmons, R.M., Finer, J.T., Chu, S. and Spudich, J.A., *Quantitative measurements of force and displacement using an optical trap* Nature, vol. 70, 1996.

[24] Antonoyiannakis, M.I. and Pendry, J.B., *Electromagnetic forces in photonic crystals* Phys.Rev.B, vol. 60, 1999.

[25] Hsu, L.C., Chen, T.C., Yang, Y.T., Huang, C.Y., Sheri, D.W., Chen, Y.T. and Lee, M., *Manipulation of micro-particles through optical interference patterns generated by integrated photonic devices* Lap Chip, vol. 13, 2013.

[26] MacDonald, M.P., Paterson, L., Sepulveda, K., Arit, J., Sibbett, W. and Dholakia, K., *Creation and manipulation of three-dimensional optically trapped structures* Science, vol. 296, 2002.

[27] Jonas, A. and Zemanek, P., *Light at work: The use of optical forces for particle manipulation, sorting and analysis* Electrophoresis, vol. 29, 2008.

[28] Ploschner, M., Cizmar, T., Mazilu, M. Di Falco, A. and Dholakia, K., *Bidirectional optical sorting of gold nanoparticles* NanoLett., vol. 12, 2012.

[29] Kippenberg, T.J. and Vahal, K.J., *Cavity opto-mechanics* Optics Express, vol. 15, 2007.

[30] Povinelli, M.L., Loncar, M., Ibanescu, M., Smythe, E.J., Johnson, S.G., Capasso, F. and Joannopoulos, J.D., *High-Q enhancement of attractive and repulsive optical forces between coupled whispering-gallery-mode resonators* Optics Express, vol. 13, 2005.

[31] Roels, J., De Vlaminck, I., Lagae, L., Maes, B., Thourhout, D.V. and Baets, R., *Tunable optical forces between nanophotonic waveguides* Nature Photon, vol. 4, 2009.

[32] Anetsberger, G., Arcizet, O., Unterreithmeier, Q.P., Rivire, R., Schliesser, A., Weig, E.M., Kotthaus, J.P. and Kippenberg, T.J., *Near-field cavity optomechanics with nanomechanical oscillators* Nature Physics, vol. 5, 2009.

[33] Woolf, D., Loncar, M. and Capasso, F., *The forces from coupled surface plasmon polaritons in planar waveguides* Optics Express, vol. 17, 2009.

[34] *Principles of Nano-Optics*(Cambridge University Press).

[35] Dholakia, K., Reece, P. and Gu, M., *Optical micromanipulation* Chem. Soc. Rev., vol. 37, 2008..

[36] Kottmann,J.P. and Martin, O.J.F., *Plasmon resonant coupling in metallic nanowires* Optics Express, vol. 8, 2001.

[37] Barnes, W.L., Dereux, A. and Ebbesen, T.W., *Surface plasmon subwavelength optics* Nature, vol. 424, 2003.

[38] Stefan Alexander Maier, *Plasmonics: Fundamentals and Applications* (Springer, United Kingdom 2007).

[39] Noguez, C., *Surface Plasmons on Metal Nanoparticles:The Influence of Shape and Environment* J.Phys.Chem., vol. 111, 2007.

[40] Garcia, M.A., *Surface Plasmons on Metal Nanoparticles:Fundamentals and Applications* Appl.Phys., vol. 44, 2011.

[41] Nordlander, P., Oubre, C., Prodan, E., Li, K. and Stockman, M.I., *Plasmon Hybridization in Nanoparticle Dimers* Nano Letters, vol. 4, 2004.

[42] Johnson, P.B. and Christy, R.W., *Optical constants of the noble metals* Phys.Rev.B, vol. 6, 1972.

[43] Zhao, R., Tassin, P., Koschny, T. and Soukoulis, C., *Optical forces in nanowire pairs and metamaterials* Optics Express, vol. 18, 2010.

[44] Zhang, H., Betremieux, Y., Noto, J. and Kerr, R., *Novel tunable liquid crystal Fabry-Perot filters for Fiber-Optical* Proceedings of SPIE, vol. 4583, 2001.

[45] Zelenina, A.S., Quidant, R., Badenes, G. and Nieto-Vesperinas, M., *Tunable optical sorting and manipulation of nanoparticles via plasmon excitation* Optics Letters, vol. 31, 2006.

[46] Sepulveda, B., Alegret, J. and Kall, M., *Nanometric control of the distance between plasmonic nanoparticles using optical forces* Optics Express, vol. 15, 2007.

[47] Liu, F., Li, Y., Wan, R., Huang, Y., Feng, X. and Zhang, W., *Hybrid coupling between long-range surface plasmon polariton mode and dielectric waveguide mode* Journal of Lightwave Technology, vol.29, 2011.

[48] Rosenberg, J., Lin, Q. and Painter, O., *Static and dynamic wavelength routing via the gradient optical force* Optics Express, vol. 17, 2009.

[49] Jiang, X., Lin, Q., Rosenberg, J., Vahala, K. and Painter, O., *High-Q double-disk microcavities for cavity optomechanics* Nature Photon, vol. 3, 2009.

[50] Ardavan, O., Pedro, A.F., Kawakami, Y. and Noda, S., *Tailoring repulsive optical force in nanophotonic waveguides* Optics Letters, vol. 36, 2011.

[51] Shun Lien Chuang, *Physics of Photonic Devices* (John Wiley Sons, 2nd edition).

Appendices

Appendix 1

FORCES IN DIPOLE APPROXIMATION

The electromagnetic force on a dipole formed by two oppositely charged particles separated by a small distance is given by

$$\mathbf{F} = (\boldsymbol{\mu} \cdot \nabla)\mathbf{E} + \dot{\boldsymbol{\mu}} \times \mathbf{B} + \dot{\mathbf{r}} \times (\boldsymbol{\mu} \cdot \nabla)\mathbf{B} \tag{A.1}$$

where $\boldsymbol{\mu}$ is the dipole moment, and $\mathbf{r}$ is the position vector pointing the center of mass of the two-body system.

To obtain time-averaged forces, we can write the second term as

$$\dot{\boldsymbol{\mu}} \times \mathbf{B} = -\boldsymbol{\mu} \times \frac{d\mathbf{B}}{dt} + \frac{d(\boldsymbol{\mu} \times \mathbf{B})}{dt} \tag{A.2}$$

$$= \boldsymbol{\mu} \times (\nabla \times \mathbf{E}) + \frac{d(\boldsymbol{\mu} \times \mathbf{B})}{dt} \tag{A.3}$$

Since the third term in the force expression is much smaller than the other two terms, it can be neglected, then

$$\mathbf{F} = (\boldsymbol{\mu} \cdot \nabla)\mathbf{E} + \boldsymbol{\mu} \times (\nabla \times \mathbf{E}) + \frac{d(\boldsymbol{\mu} \times \mathbf{B})}{dt} \tag{A.4}$$

Time averaging the equation 2.24, the last term vanishes, the resulting time-

averaged force is

$$\langle \mathbf{F} \rangle = \sum_i \langle \mu_i(t) \nabla E_i(t) \rangle \tag{A.5}$$

Now, we consider a dipolar particle illuminated by a monochromatic electromagnetic wave for which the time dependende can be given simply by $exp(-i\omega t)$ added to $\mathbf{E}(\mathbf{r}, \mathbf{t})$ and $\mathbf{B}(\mathbf{r}, \mathbf{t})$. Similarly, the dipole will have same time dependent part.

The induced dipole moment in the particle is given by

$$\boldsymbol{\mu} = \alpha(\omega)\mathbf{E} \tag{A.6}$$

where α is polarizability of the particle.

The time- averaged force using equation 2.21, and neglecting last term, is given by

$$\langle \mathbf{F} \rangle = \frac{1}{2} Re(\boldsymbol{\mu}^* \cdot \nabla)\mathbf{E} - i\omega(\boldsymbol{\mu}^* \times \mathbf{B}) \tag{A.7}$$

Then,

$$\langle \mathbf{F} \rangle = \frac{1}{4} \nabla(\boldsymbol{\mu}^* \cdot \acute{\mathbf{E}} + \boldsymbol{\mu} \cdot \acute{\mathbf{E}}^*) \tag{A.8}$$

where ∇ acts only on $\mathbf{E}'$. We can write complex electric field as

$$\mathbf{E}(r) = E_0(r) exp(i\phi(r))\mathbf{n_E} \tag{A.9}$$

where $\mathbf{n_E}$ is the unit vector in the direction of polarization, $\phi(r)$ is the phase and E_0 is the real amplitude.

We end up with the time-averaged force in terms of complex polarizability $\alpha = \alpha' + i\alpha''$ and electric fields as follows

$$\langle \mathbf{F} \rangle = \frac{\alpha'}{4} \nabla E_0^2 + \frac{\alpha''}{2} E_0^2 \nabla \phi \tag{A.10}$$

Here, the first term is the gradient force which arises from the gradient of the field. The second term corresponds to scattering force which is proportional to the imaginary part of the polarizability. The scattering force exist due to the momentum transfer from the radiation field to the particle.

Appendix 2

COUPLED MODE THEORY

The conventional coupled mode theory is mainly based on the modes of the individual uncoupled waveguides. The simplest model for the coupled-waveguide system is a directional coupler consisting of two uniform, parallel waveguides which are sufficiently close such that their fields overlap. We consider guided modes along the x-direction of two rectangular dielectric waveguides to have implicit time dependence $exp(jwt)$. When the waveguides are infinitely far apart, they are uncoupled. In the case of coupling, the total fields can be written as linear combinations of the individual waveguide modes as given in [51]

$$E = a(x)E^{(1)} + b(x)E^{(2)} \tag{B.1}$$

$$H = a(x)H^{(1)} + b(x)H^{(2)} \tag{B.2}$$

The variation of amplitudes $a(z)$ and $b(z)$ satisfy

$$\frac{da}{dx} = i\beta_a a + iK_{ab}b \tag{B.3}$$

$$\frac{db}{dx} = iK_{ba}a + i\beta_b b \tag{B.4}$$

where K_{ab} and K_{ba} are mutual coupling coefficients, β_a and β_b are the propagation constants of individual waveguides.

The total guided power is

$$P(z) = |a(x)|^2 + |b(x)|^2 + Re[a(x)b^*(x)C_{ba} + b(x)a^*(x)C_{ab}] \tag{B.5}$$

where C_{ab} and C_{ba} are cross overlap integrals. If the coupling is weak, the cross overlap integrals are negligible, and for the lossless system the total power obeys

$$P(z) = |a(x)|^2 + |b(x)|^2 \tag{B.6}$$

$$\frac{dP(x)}{dx} = 0 \tag{B.7}$$

The coupled mode equations can be written in a matrix form

$$\frac{d}{dx}\begin{bmatrix} a \\ b \end{bmatrix} = i\bar{H}\begin{bmatrix} a \\ b \end{bmatrix} \tag{B.8}$$

where $H = \begin{bmatrix} \beta_a & K_{ab} \\ K_{ba} & \beta_b \end{bmatrix}$.

The eigenstate solutions can be found by

$$\begin{bmatrix} a(x) \\ b(x) \end{bmatrix} = \begin{bmatrix} A \\ B \end{bmatrix} exp(i\beta x) \tag{B.9}$$

and there are two eigenvalues for β:

$$\beta_s = \frac{\beta_a + \beta_b}{2} + \psi \tag{B.10}$$

$$\beta_a = \frac{\beta_a + \beta_b}{2} - \psi \tag{B.11}$$

where

$$\delta = \frac{\beta_b - \beta_a}{2} \tag{B.12}$$

$$\psi = (\delta^2 + K_{ab}K_{ba})^{1/2} \tag{B.13}$$

The corresponding eigenvectors are

$$v_1 = \begin{bmatrix} K_{ab} \\ \delta + \psi \end{bmatrix} \tag{B.14}$$

$$v_2 = \begin{bmatrix} K_{ab} \\ \delta - \psi \end{bmatrix} \tag{B.15}$$

The solutions can be expressed by a matrix $\bar{S}$ and the initial conditions

$$\begin{bmatrix} a(x) \\ b(x) \end{bmatrix} = \bar{S} \begin{bmatrix} a(0) \\ b(0) \end{bmatrix} \tag{B.16}$$

$$\bar{S} = \begin{bmatrix} cos\psi x - i\frac{\delta}{\psi} sin\psi x & i\frac{K_{ab}}{\psi} sin\psi x \\ i\frac{K_{ba}}{\psi} sin\psi x & cos\psi x + i\frac{\delta}{\psi} sin\psi x \end{bmatrix} e^{i(\beta_a+\beta_b)x/2} \tag{B.17}$$

We assume that initially only the first waveguide is excited, e.g. $a(0) = 1, b(0) = 0$, and if $\beta_a = \beta_b$, the solutions are

$$a(x) = cosKxe^{i\beta x} \tag{B.18}$$

$$b(x) = isinKxe^{i\beta x} \tag{B.19}$$

where $K = K_{ab} = K_{ba}$ and $\beta = \beta_a = \beta_b$

An important parameter of the coupling is the power length L_c at which maximum power transfer from the excited waveguide to the second coupled waveguide will occur. The coupling length is given by

$$L_c = \frac{\pi}{\beta_s - \beta_a} \tag{B.20}$$

where β_s and β_a denote the symmetric (even) and the antisymmetric(odd) propagation constants.

VITA

Aybike Ural Yalçın was born in Istanbul in 1988. After graduating high school in Özel talyan Lisesi, she started undergraduate study in Işık University in 2006. She received her B.Sc. degree in 2011 and has been accepted to M.Sc. program in the Koç University. She started the research under the supervision of Assist.Prof. Kaan Güven. From September 2011 to August 2013 she worked as a teaching assistant in Koç University. She is currently working on the optical forces in plasmonic nanostructures and waveguides and she will continue her Ph.D. studies at Koç University.